Using Patterned Arrays of Metal Nanoparticles to Probe Plasmon Enhanced Luminescence of CdSe Quantum Dots

Yang-Hsiang Chan,[†] Jixin Chen,[†] Stacey E. Wark, Stephanie L. Skiles,[‡] Dong Hee Son,* and James D. Batteas*

Department of Chemistry, Texas A&M University, P.O. Box 30012, College Station, Texas 77842-3012, [†]Both authors contributed equally to this work. [‡]Ms. Skiles was an NSF-REU student from the Department of Chemistry, Wayland Baptist University, 1900 W. 7th Street, Plainview, TX 79072 during the summer of 2008

ABSTRACT Here we present a simple platform for probing plasmon enhanced photoluminescence (PL) of quantum dots by confocal microscopy. In this study, self-assembled monolayers of silane-derivative molecules were patterned onto the oxidized GaAs surfaces to direct the attachment of Au or Ag nanoparticles onto the surface. Following the directed binding of metal nanoparticles (MNPs), a layer-by-layer deposition of oppositely charged polymers was used to create films with varying thickness by controlling the numbers of deposited layers. CdSe quantum dots (QDs) of ~4 and 5.5 nm in diameter with 16-mercaptohexadecanoic acid as a surfactant were then adsorbed onto the outermost polymer layer *via* electrostatic interactions. Using confocal fluorescence microscopy, the enhanced PL from the CdSe over the Au or Ag nanoparticle patterns could be imaged directly and scaled against the regions with no Au or Ag nanoparticles, and the luminescence of the GaAs (as an internal standard) for different CdSe—metal separations. By using a pattern, PL enhancement as a function of particle-CdSe spacing can be readily probed all on a single platform, where the QDs over MNPs and not over MNPs can be directly compared in the same dielectric environment. The observed luminescence as a function of metal-QD separation can be readily fit to a combined model of metal—fluorophore fluorescence quenching and local electric field enhancement.

KEYWORDS: CdSe · patterning of metal on GaAs · metal nanoparticle enhanced fluorescence · fluorescence resonance energy transfer (FRET) · nanosurface energy transfer (NSET)

It is well-known that the local surface plasmon resonance (LSRP) of metal nanoparticles (MNPs) can be excited when the particles are optically irradiated. The energy of the surface plasmon resonance is found to be dependent on the size, shape, composition, and organization of the metal nanostructure. As the LSPR of MNPs is found to change in response to the dielectric environment surrounding the particles, shifts in the peak position of the LSPR can be followed as a means of detection of analytes.[1,2] Enhancement in the Raman scattering of molecules in the proximity of MNPs have also been reported, which gives rise to surface enhanced Raman spectra (SERS) for which detection of signals down to the single molecule level have been reported.[3,4] Related to this, it has been observed that the photoluminescence intensity of quantum dots (QDs) and quantum wells (QWs) can also be enhanced by the electromagnetic coupling with metal surface plasmons.[5−11] Time-resolved spectroscopic studies of QD and QW structures coupled to MNPs have shown that the radiative decay rate, absorption cross section, and quantum efficiencies of luminescence generally increase in the presence of metal nanostructures due to the increased local electric field surrounding the irradiated metal structures. For example, Atwater and co-workers have shown that for Si nanocrystals coupled with a rough Au film, that the quantum efficiency for luminescence could be increased by *ca.* 60%.[9] The extent of the enhancement that can be achieved by coupling of QDs to metal nanostructures or rough films, strongly depends on the proximity of the QDs to the metal structure, and has been shown to decay exponentially with increasing distance between the two. By bringing QDs closer to the metal, their photoluminescence can be enhanced by the locally increased electric field. However, if the QDs are too close to the MNP, quenching of the photoluminescence is observed. As such, a maximum in photoluminescence enhancement is found to occur at an optimal separation depending on the competitive effects of the distance dependence of the electric field and the quenching efficiency. In addition to QD-particle separation, the structure and type of metal particles used (*e.g.*, Ag, Au), polarization of the incident light, and the laser

*Address correspondence to batteas@mail.chem.tamu.edu, dhson@mail.chem.tamu.edu.

Received for review March 30, 2009 and accepted May 24, 2009.

Published online June 5, 2009.
10.1021/nn900317n CCC: $40.75

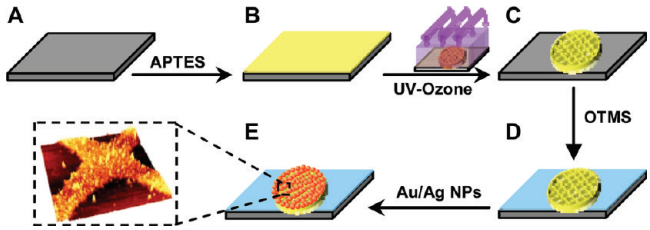

Scheme 1. Schematic diagram of patterning metal NPs on GaAs. GaAs substrates are first cleaned and oxidized (A), and then modified with an APTES SAM (B). A Cu TEM grid is placed on top of SAM-functionalized GaAs surface and exposed to the UV-ozone for 20 min, leaving an APTES SAM in the unexposed regions (C). After removing the grid, the GaAs surfaces are immersed in OTMS solutions for 4 h to backfill the excavated area (D). The substrates are next soaked in the desired citrate stabilized Au or Ag NPs aqueous solution where they attach to the amine terminated regions of the surface (E).

power have all been found to influence the extent of plasmon enhanced photoluminescence. The ability to quantitatively determine the extent of photoluminescence enhancement as a function of QD-metal separation however can be challenging as artifacts such as scattering differences between samples, variations in laser intensity, and differences in dielectric medium can make scaling the luminescence intensities of coupled and noncoupled quantum dots difficult to evaluate.

In this paper we present a simple platform in which the coupling of CdSe quantum dots with Au or Ag nanoparticles has been quantitatively measured. To address some of the above-mentioned challenges, we have positioned a single layer of quantum dots on top of arrays of the desired metal nanostructure positioned in a grid pattern, in which the separation between the two was controlled with a polymer spacer formed using layer-by-layer assembly. This simple approach yields a patterned structure in which the photoluminescence of the QDs above the metal patterns may be directly scaled against those not above the metal pattern by imaging the structure with confocal fluorescence microscopy. Additionally as this structure is built on a GaAs(100) single crystal, the inherent luminescence of the GaAs offers the means of scaling each measurement from sample to sample, aiding in eliminating effects of scattering or variations in laser intensity. From these studies we have shown that this simple platform can be readily made using chemical self-assembly approaches and adapted to various materials. Here we report two initial studies of the coupling of CdSe quantum dots of *ca.* 4 and 5.5 nm in diameter, with Au nanoparticles and Ag nanoprisms, respectively, as a function of metal-QD separation.

RESULTS AND DISCUSSION

Formation of Au or Ag Arrays on GaAs. To directly compare the effects of metal nanoparticles on the photoluminescence of QDs, we created a patterned array of metal nanoparticles on a GaAs substrate by directing attachment of the metal particles to the surface with an amine-terminated self-assembled monolayer. This patterned layer could then be covered by a polymer spacer layer of varying thickness through layer-by-layer assembly and then coated with a single layer of quantum dots. Using this approach the ratio of the photoluminescence intensities from the QDs over the metal particles could be directly scaled against the regions without metal particles in a single photoluminescence image. Scheme 1 illustrates our method of selectively patterning Au or Ag nanoparticles (NPs) on the GaAs surface. While several approaches were tried (see Supporting Information), ultimately the attachment of alkoxysilane SAMs on the oxidized GaAs surface yielded the best results in terms of film stability and metal particle attachment density.

To form the patterned metal grid structure, the cleaned and oxidized GaAs surface was first coated with a uniform SAM of the aminopropyltriethoxysilane (APTES) (Scheme 1B). Following APTES assembly, a Cu TEM grid was placed in conformal contact with the GaAs substrate to function as shadow mask, and the sample was then exposed to UV/ozone to photooxidize the uncovered portions of the SAM layer (Scheme 1C). Following rinsing, the oxidized SAM was removed and now the uncovered GaAs regions were then backfilled with an octadecyltrimethoxysilane (OTMS) SAM resulting in a patterned array of hydrophilic and hydrophobic regions on the surface (Scheme 1D). Finally, the sample was immersed in the desired solution of Au or Ag NPs (*ca.* pH 7) to allow for the citrate stabilized NPs to attach onto the amine rich regions by electrostatic interaction (Scheme 1E). A few nanoparticles were found to attach to the OTMS regions, but those that did were weakly bound and could be readily rinsed away.

As the assembly process was carried out in water, the stability of the SAM is of the utmost importance. To confirm the high quality and stability of the silane SAMs formed using this method, Fourier transform infrared reflection absorption spectroscopy (FT-IRAS) measurements were obtained for OTMS SAMs and XPS experiments were performed for the APTES SAMs on the oxidized GaAs surface. The FTIR spectra of OTMS sample showed that the $\nu_{as}(CH_2)$ asymmetric stretch was centered around 2917 cm^{-1} (data not shown), which is characteristic of well-ordered crystalline-like silane SAM.[12,13] After 8 months of air exposure, the OTMS SAMs were observed to exhibit no observable signal decrease for both $\nu(CH_2)$ and $\nu(CH_3)$ stretch modes and the $\nu_{as}(CH_2)$ asymmetric stretch was maintained at *ca.* 2917 cm^{-1}. As compared to SAMs of octadecanethiol on GaAs, which we also explored for this patterning purpose (see Supporting Information), these films demonstrated much greater stability, as the octadecanethiol/GaAs SAMs were found to degrade within a couple of weeks under ambient conditions. For the APTES SAMs, a representative survey spectrum of XPS that is shown in Figure 1 confirms the presence of the APTES SAM on

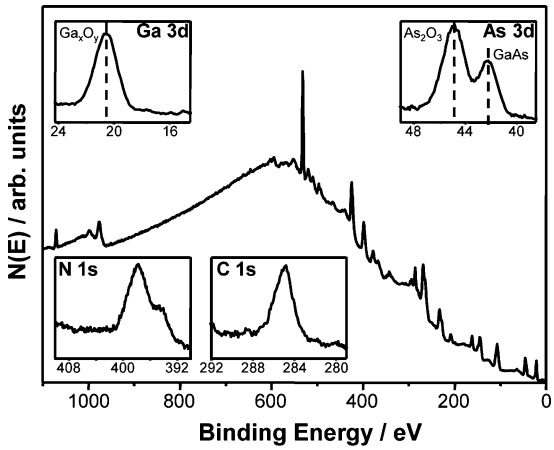

Figure 1. X-ray photoelectron survey and high-resolution spectra for APTES monolayers on GaAs (100). The high-resolution spectra show the Ga(3d), As(3d), N(1s), and C(1s) spectral regions which show that the surface is first oxidized and then covered by the APTES SAM.

the oxidized GaAs surface. High-resolution spectra of the C(1s), N(1s), and Ga(3d) regions show peak binding energies of 284.8 ± 0.1, 399.0 ± 0.1, and 20.5 ± 0.1 eV, respectively, while the high-resolution As(3d) signal can be separated into two peaks at 44.8 ± 0.1 for As oxides and 42.2 ± 0.1 eV corresponding to GaAs bulk. The XPS data also indicate that a fresh oxidation layer was readily introduced by UV/ozone and the APTES monolayers were successfully grown on these surfaces.

Following particle attachment, the resulting grid structures were examined by AFM. Topographic AFM images of the patterned Au arrays on GaAs are shown in Figure 2A−D. The cross-sectional profile (Figure 2B) reveals that the average height of the Au array is 18 ± 2 nm which is consistent with the size of single-layer Au NPs, suggesting that the interparticle repulsive force due to the citrate stabilizer was sufficient to prevent the physical adsorption of a second layer of Au NPs. Similar results were also observed for Ag-nanoprism patterns as presented in Figure 2E−H, in which the cross-sectional analysis shows the average height of ~120 nm in accordance with the edge-length of a silver nanoprism, suggesting the Ag nanoprisms stand up face by face rather than lie down flat and stack on the surface. As mentioned above, the gold nanoparticles were found to exhibit an absorption maximum at ~523 nm, which suggests that the average size is ~18 nm in diameter.[14] The silver nanoprisms of 100 ± 20 nm in edge-length, which were synthesized from small Ag nanospheres following the reported photoinduced transformation method,[15] have two broad absorption peaks around 450 and 670 nm. The extinction spectra of each however were found to be modified after deposition onto the substrate (determined from deposition on APTES modified glass coverslips) showing the emergence of an extinction peak at 660 nm for gold NPs and the broadening of silver-NP plasmon peak at higher wavelength. These effects can be ascribed to interparticle coupling and/or disorder of the NP films (Figure 3).[16,17] These interparticle coupling effects will impact the PL enhancement of QDs based on the degree of spectral overlap as has been reported previously.[8,18,19]

Controlling CdSe−Metal Distance. Previous work by Kulakovich *et al.* has shown that layer-by-layer polymer assembly can be used to provide a controllable spacing layer for QD-metal films. Here we have adapted this approach to our patterned array to also control separation and test our platform against a known system (CdSe−Au).[7] Following creation of the metal grid structure, the CdSe quantum dots of the desired size were then attached at controlled distances from the metal pattern using layer-by-layer polymer assembly. Here, alternating layers of poly(diallyldimethylammonium chloride) (PDADMAC) and poly(sodium 4-styrenesulfonate) (PSS) were put on the surface in order to build up films

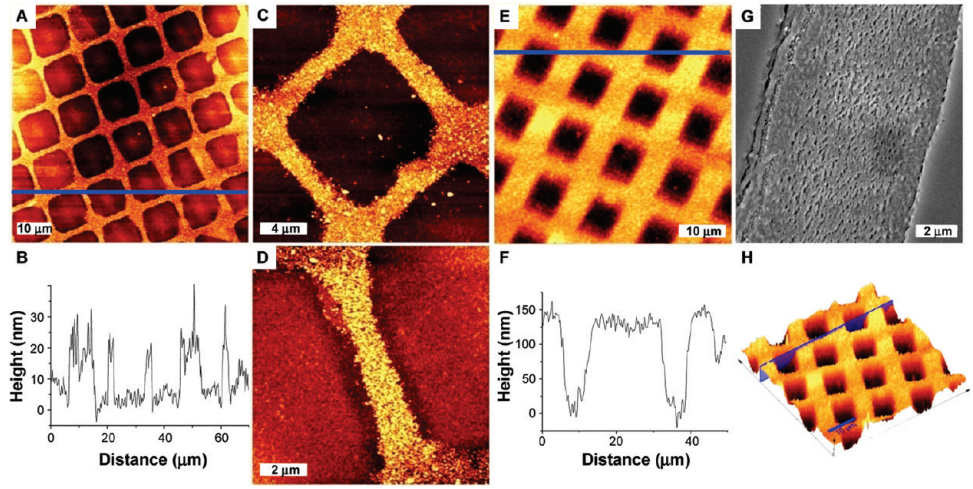

Figure 2. Topographic AFM images of the Au and Ag patterned metal nanoparticle arrays on GaAs(100). Au−NP patterns: (A) 70 × 70 μm² and (B) its corresponding cross-sectional plot (blue line) showing that a single layer of particles is bound to the surface, (C) 20 × 20 μm², and (D) 10 × 10 μm². Ag−NP patterns: (E) 50 × 50 μm² and (F) its corresponding cross-sectional plot (blue line). (G) SEM image (10 × 10 μm²) of the Ag film and a (H) 3-D topographical plot showing the waffle-like structure of the thick Ag film which corresponds in thickness to the long axis of the Ag nanotriangles used.

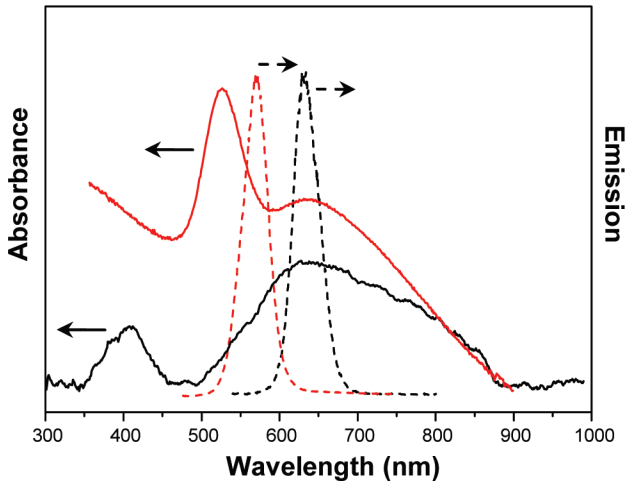

Figure 3. UV−visible spectra of Ag NPs (solid black line) and Au NPs (solid red line) on APTES-modified glass with five layers of PSS: PDADMAC; and photoluminescence of 5.5 nm CdSe (dash black line) and 4 nm CdSe (dash red line) nanocrystals on top of five layers of PSS:PDADMAC.

of controlled thickness. This began with a positively charged layer of PDADMAC, followed by the negatively charged PSS layer. Terminating with an additional PDADMAC layer yields a surface with a net positive charge, onto which our 16-MHA terminated CdSe particles (which carry a net negative charge at the assembly pH) could then be bound electrostatically (Figure 4A). Importantly, these types of polymer layers have no optical absorption in the visible region of the spectrum and have not been reported to quench QD photoluminescence.[7,20] Although the thickness dependence of these different polyelectrolyte layers has been well determined previously[21] for deposition on surfaces such as polystyrene particles, it is likely that this will dramatically vary from surface to surface. As such, to accurately determine the polymer film thickness, in our patterned arrays, a background thickness (D_1) was determined by tapping-mode AFM after slightly scratching through assembled polymer films with varying numbers of layers on the oxidized GaAs surface (Figure 4). Extending this to the patterned grid such as for the Au−NP system, illustrated in Figure 4A, once the value of D_1 is determined, the thickness of polymer thin films above Au NPs, D, can be simply derived from the following relationship:

$$H + 4 + D_1 = 4 + D + 18 \text{ (nm)} \qquad (1)$$

where 4 nm is the average diameter of the CdSe QDs, 18 nm is the average diameter of the Au nanoparticles, and H is the height difference between the regions with and without Au NPs after coating of the polyelectrolyte spacers and CdSe QDs, as determined from the topographic AFM images (*e.g.*, Figure 5A). Plotting the value, D_1, against different numbers of polymer layers (Figure 4C) shows a nonlinear increase in film thickness with the number of layers.

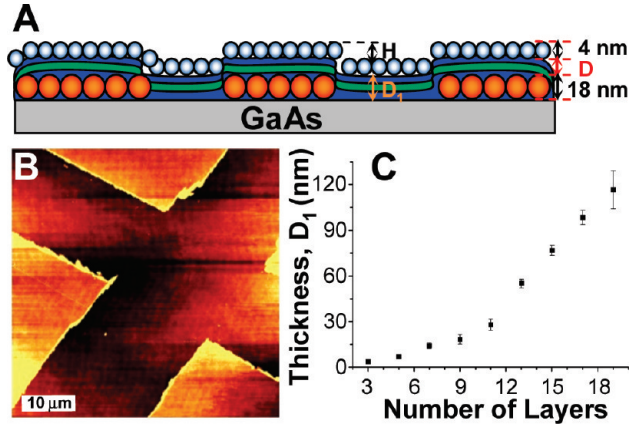

Figure 4. (A) Schematic cross-sectional view of the sample showing that polymers and 4 nm QDs were deposited onto Au-NP arrays on GaAs in sequence. (B) AFM topographic image of different layers of polymers deposited on pure GaAs substrates without metal patterns which were removed by scratching. (C) The polymer thickness on bare GaAs (D_1) measured from AFM *versus* the number of polyelectrolyte layers.

Photoluminescence Measurements. By using patterns of Au or Ag NPs on the GaAs surface, the environment of the CdSe QDs could be separated into two parts: regions with and without NPs under the polymer spacer layer. To measure the relative photoluminescence of the two regions, the sample was imaged using a confocal fluorescence microscope with an Ar ion laser at 488 nm as the excitation light. The PL intensity of CdSe over the NPs could then be directly normalized to those of the adjacent CdSe without NPs. Figure 5B shows a typical luminescence spectrum within this ensemble. The peak around 585 nm originates from CdSe QDs and the peak around 845 nm is from the GaAs background. Although the PL intensity from the GaAs background should remain constant during each experiment, undesired fluctuations of laser power can occur from sample to sample. Thus, by using GaAs as the support background, we could use the PL intensity from GaAs as a built-in reference to normalize the PL intensity of the QDs for each individual measurement. A representative PL image plotted using the CdSe emission spectrum, integrated from 500−650 nm clearly shows that the luminescence of the QDs over the Au pattern is enhanced relative to the nonmetal containing regions (Figure 5C). From the cursor profile (Figure 5D) it can be seen that in this case the QDs over the metal particles show nearly twice the intensity of those not over the metal.

One challenge in quantifying the extent of the photoluminescence enhancement is that reflection or scattering of the laser source by the MNPs might re-excite the CdSe QDs and thus results in an artificial increase in CdSe PL. To examine the possibility of this factor, the sample was scanned with a low laser power (70 nW/μm^2) and a confocal scanning image was generated by collecting the 488 nm laser spectrum itself (Figure 6A). The results indicate that the gold NPs strongly absorb the laser light owing to their broad absorption

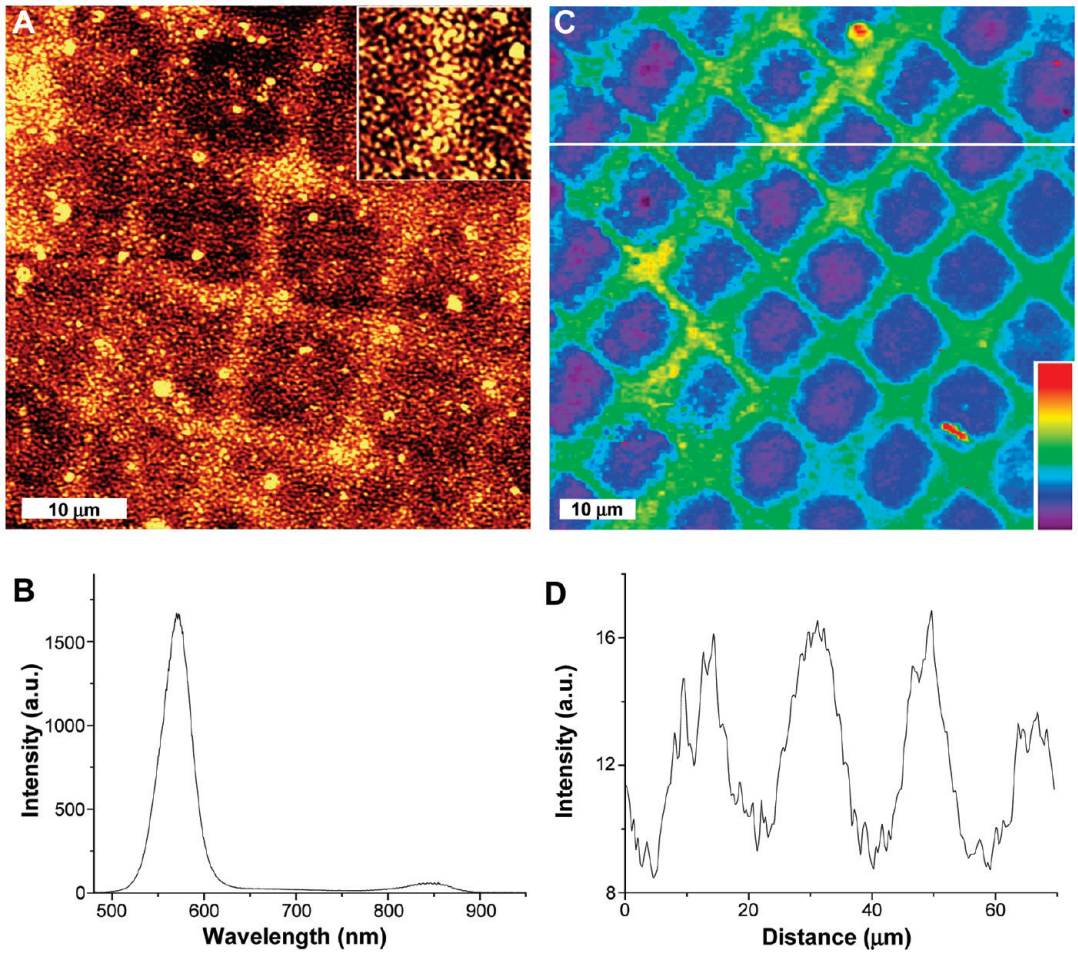

Figure 5. (A) Topographic AFM image of CdSe QDs deposited on 19 layers of polymer over a Au-NP patterned GaAs surface. The top-right inset magnifies a 10 × 10 μm² area. (B) A representative emission spectrum from the film in panel A shows both the CdSe and GaAs emission at *ca.* 585 and 845 nm, respectively. (C) A false color photoluminescence image of 4 nm CdSe QDs above nine layers of polymers on Au-NP patterned GaAs surfaces (the *z*-scale bar is from 7−23 au). The image is produced by integrating the spectral region for the CdSe from 500−650 nm. (D) The cross-sectional plot corresponds to the white line in panel C, illustrating the relative photoluminescence enhancement.

around 523 nm rather than reflect/scatter the laser light. As shown in Figure 6B, the laser intensity above the regions of Au NPs (white spot) shows 48% lower intensity than that above the regions without Au NPs (red spot). Nevertheless, based on this, the relative absorption is insignificant and can be neglected when higher laser powers (*ca.* several tens of μW/μm²) are used for the PL measurements. Similar results for PL enhancement of CdSe QDs of 5.5 nm in diameter were observed on Ag-NP arrays (Figure 7).

The plasmon enhancement of the QD photoluminescence was found to depend on the number of polymer layers which controls the QD-metal separation (Figure 8). For the Au−NP system, the enhancement was found to reach a maximum at nine layers of polymer, corresponding to ~10.8 nm. For the Ag-NP system, the maximum peak was at five layers of polymer (~7.7 nm). An overall maximum enhancement by a factor of 2 was observed in both the CdSe−Au and CdSe−Ag systems, and is consistent with previous results for coupling between CdSe and Au nanoparticles.[7] These results can be partially attributed to the locally enhanced electric field surrounding the MNPs under illumination, where the maximum field enhancement should oc-

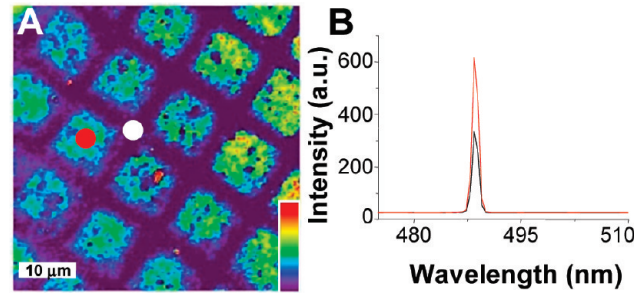

Figure 6. (A) A confocal scanning microscopy image generated by collecting the 488 nm laser line on nine layers of polymers deposited upon Au-NP patterned GaAs surfaces (the *z*-scale bar is from 50−850 au). (B) Spectra on the GaAs background (red circle) and Au-NP patterned (white circle) regions. The red line and the black line represent the averaged spectrum of the reflected laser light of red circle and white circle areas in panel A, respectively.

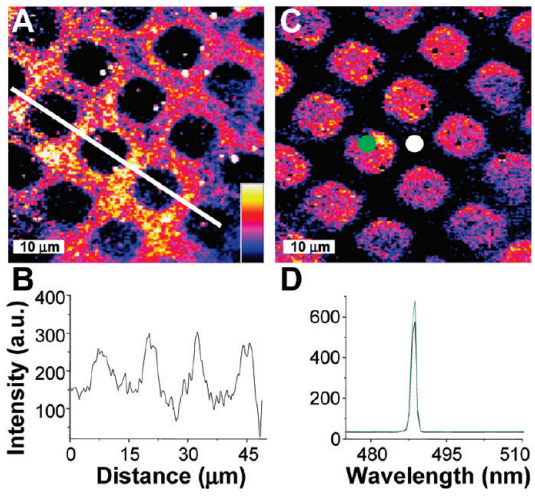

Figure 7. (A) False color photoluminescence image of 5.5 nm CdSe QDs above five layers of polymer on a Ag-NP patterned GaAs surface (the *z*-scale bar is from 165−300 au) and (B) its cross-section analysis along the white line. (C) The corresponding confocal image at the same scanning region generated by collecting the 488 nm laser line on five layers of polymers deposited upon Ag-NP patterned GaAs surfaces. (D) Reflected laser light from the GaAs background (green circle) and the Ag-NP patterned (white circle) regions. The green line and the black line represent the averaged spectrum of green circle and white circle areas in panel C, respectively.

cur at the closest QD-metal separation distance.[22] At such close QD-particle distances however competitive mechanisms such as quenching prevail due to electron transfer or nonradiative energy transfer from the QDs to the metal.[23−27] As such, these two mechanisms compete with each other and thus render a distribution of PL enhancement as a function of separation between the QDs and MNPs (Figure 8). When the QDs are more than 20 nm away from the MNPs, there is little to no coupling observed between the QDs and the MNPs. For the CdSe−Au system, the trend in photoluminescence enhancement as a function of distance was found to be highly reproducible. For the CdSe−Ag system, however, a large standard deviation in the photoluminescence intensity was observed for small separations. We attribute this to the much larger surface corrugation of the Ag films, due to the much larger particles and degree of inhomogeneity in their size (~100 ± 20 nm).

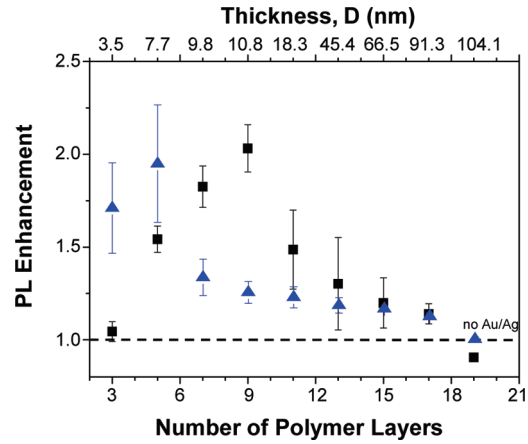

Figure 8. PL intensity enhancement of CdSe QDs *versus* number of polymer layers between QDs and Au (black squares)/Ag (blue triangles) NPs. The upper *x*-axis indicates the calibrated thickness of corresponding polymer spacer (*D*) above metal NPs as illustrated in Figure 4A.

While the measured enhancement for the CdSe−Au was consistent with previous reports, the observed enhancement for the Ag system was lower than we expected considering the typically large enhancements for other optical properties such as SERS signals for Ag as compared to Au materials. In one previous report, coupling between InGaN with rough Ag films was shown to yield enhancements by as much as 14-fold.[8] One might also expect that Ag nanoprisms should offer higher enhancement than the Au nanoparticles because the larger local electric field typically surrounds the sharp points of a Ag nanoprism. Several factors may contribute to the lower than expected enhancement. In particular, our yield of complete photoinduced conversion of Ag nanospheres to nanoprisms was found to be only ~50% on the basis of the UV−visible spectra and TEM images (Supporting Information, Figure S2), such that *ca*. half of the Ag NPs in the films are nonresonant with both the CdSe QDs as well as the excitation laser. The intrinsic low-coverage of citrate-coated Au or Ag NPs on the surfaces may also partially explain the lower than expected enhancement.[28] Lastly, it has also been demonstrated that the angle of the incident light and polarization can greatly influence the local-field enhancement for materials with sharp geometries such as nanoprisms, which we did not vary in our measurements.[17,29] As such, each of these factors likely contribute to the reduced PL enhancement by the citrate-covered Ag nanoprisms.

Mechanism. To elaborate on the experimental results to determine if the distance dependence we observed is reasonable, we separated the interactions between QDs and MNPs into two factors: PL quenching due to energy transfer from the QDs to the MNPs and the electric field induced PL enhancement from MNPs on the QDs. Here, due to the complexity of the CdSe−Ag system, we will only examine the CdSe−Au system. Based on the competing factors of quenching and electric field enhancement, the final apparent enhancement of the PL intensity can be depicted as

$$\frac{I}{I_0} = P_Q \times P_E \qquad (2)$$

Where I is the PL intensity of QDs over the MNP-coated GaAs surface; I_0 is the PL intensity of QDs without MNP coupling; P_Q and P_E are the quenching factor and enhancement factor, respectively, as described in eqs 3 and 4 later. For the PL quenching part, an energy

transfer mechanism has been successfully employed in various systems including dye−dye, MNP−dye, and QD−dye platforms.[30−32] To simplify our system, we will assume that for each QD there is only one MNP nearby. It should be noted that experimentally, based on the average surface coverage of the QDs and metal nanoparticles determined by AFM measurements, that there are *ca.* three to four QDs per Au particle. On the basis of the relative particle sizes and their average surface coverage, statistically this ratio yields nearly one QD per MNP in close enough proximity to experience PL enhancement. The next closest QDs would be *ca.* 40 nm from a MNP, and based on our measurements may contribute *ca.* 20% to the measured PL enhancement. Under these conditions, the PL quenching factor can be written as[27,33,34]

$$P_Q = \frac{(d/R_Q)^{n_Q}}{1 + (d/R_Q)^{n_Q}} \quad (3)$$

where d is the MNP−QD separation distance; R_Q is the Förster like radius at which 50% of the fluorescence is quenched; n_Q is the dependence of fluorescence quenching on the MNP−QD separation distance. For the Förster dipole−dipole energy transfer or fluorescence resonance energy transfer (FRET) mechanism,[30] the energy transfer quenching exhibits an $(d/R_Q)^6$ dependence. While for other mechanisms such as the nanosurface energy transfer (NSET) process, n_Q will equal 4.[27,35,36] Yun *et al.* has claimed to be able to distinguish between FRET and NSET processes by controlling the distance between a Au NP and a dye.[33] As such, by fitting our photoluminescence enhancement data we will also attempt to do the same.

For the PL enhancement part, it has been theoretically and experimentally demonstrated that the enhancement efficiency depends on the spectral overlap between donor emission and LSPR of MNPs and is proportional to the near field electric field intensity of the metal surface.[37−39] Here, we simplify the enhancement model *via* the following equation:

$$P_E = \left(\frac{R_E}{d}\right)^{n_E} + 1 \quad (4)$$

where R_E is a constant for the MNP−QD separation at where we observe twice the luminescence enhancement, d is the same MNP−QD separation distance in eq 3, and n_E is the distance dependence power.

To apply these models to our data, the experimental data of the Au−QD system (Figure 8) was fit using eq 2, combined with eqs 3 and 4, where n_Q was set to 4 or 6 and R_Q was calculated directly for either the FRET or NSET models based on the materials (see Supporting Information). All of the other parameters, d, R_E, and n_E, were left to be freely variable in the fit. If the fit to the data is better for $n_Q = 4$, this would suggest that the NSET mechanism dominates the energy transfer quenching processes. However, if a better fit is obtained for $n_Q = 6$, this would be indicative of a FRET mechanism being the major contributor to the quenching of the QD PL. The fitting of our results for both $n_Q = 4$ and 6 are shown in Figure 9, in which the green and blue dashed lines represent the curves for quenching and electric field enhancement as a function of MNP−QD separation distance, respectively. From these results, it can be seen that when $n_Q = 6$ a much better fit to the data is found, suggesting that the FRET mechanism seems to dominate in our system. This finding is consistent with earlier studies of ZnS capped CdSe coupled to Au nanoparticles *via* peptide tethers.[27]

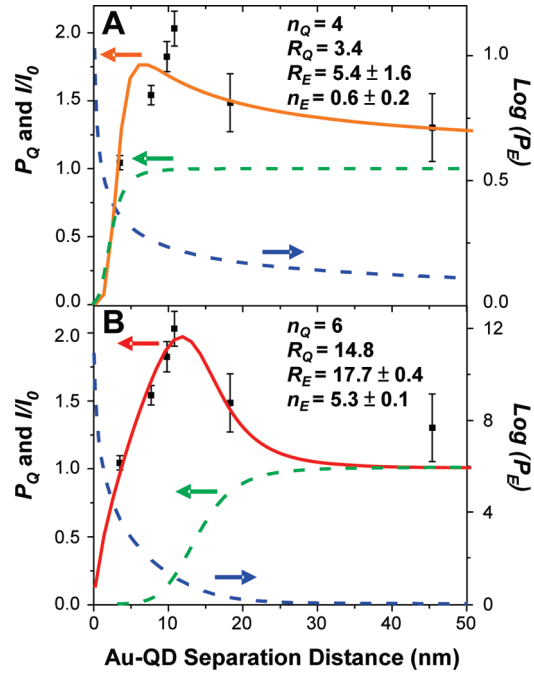

Figure 9. Fitting results for PL intensity enhancement for the Au−QD system for (A) $n_Q = 4$ and (B) $n_Q = 6$. The data points are from Figure 8. Only 0−50 nm of separation is shown to highlight the fit near the peak position. The orange and red solid lines represent the apparent PL enhancement as described in eq 2 for the NSET and FRET mechanisms. The green and blue dashed curves depict the quenching and enhancement factors as described in eqs 3 and 4, respectively.

CONCLUSIONS

Using a patterned array of metal particles, photoluminescence enhancement for CdSe coupled to Au nanoparticles and CdSe coupled to Ag nanoprisms was investigated as a function of the CdSe-metal separation distance. The use of a patterned array allowed for the photoluminescence enhancement to be readily scaled between regions with and without metal particles and account for any scattering or differences in dielectric medium that could influence the determination of the relative enhancement, all in a single experiment. The PL enhancement of CdSe coupled to

Au and Ag particles was found to peak at a factor of 2 at distances of ~11 and 8 nm, respectively. The resulting data can be explained by the competition between energy transfer quenching and plasmon-assisted enhancement of the QD photoluminescence and could be fit to a simple model combining these two effects. This simple platform which can be fabricated using directed assembly approaches should be readily adaptable to probing photoluminescence enhancement for a range of other materials.

METHODS

Preparation of Silane Monolayers. Single side polished GaAs(100) substrates (AXT, 400 μm, Si-doped, University Wafer, Inc., Boston, MA) were etched and cleaned following the procedures described previously by Jun *et al*. to remove the native oxide using dilute acid and base solutions.[40] Briefly, the GaAs samples were immersed into 1:20 NH_4OH/H_2O solution for 1 min and then rinsed liberally with high purity (18.2 MΩ · cm) water (NANOpure Diamond, Barnstead), followed by ethanol. The GaAs substrates were immediately immersed into a 1:10 HCl/ethanol solution for 1 min. The substrates were subsequently rinsed with copious ethanol, blown dry with streaming nitrogen, and treated with UV/ozone for 20 min to make a fresh oxide layer on the GaAs surfaces. Self-assembled monolayers (SAMs) of 3-aminopropyltriethoxylsilane (APTES, purchased from Gelest, Inc.) were formed by immersion of the freshly oxidized GaAs substrates in 5 mM APTES in ethanol for 12 h. After being taken out from the solution of APTES, the SAM-modified substrates were rinsed with ethanol and blown dry under a nitrogen stream in preparation for patterning. AFM measurements of these films suggest that only a monolayer is formed on the oxidized GaAs surface as no domain structures are observed and the film exhibit the same roughness as the underlying surface.

X-ray Photoelectron Spectroscopy. To evaluate the surface chemistry XPS data were acquired with a Kratos Axis ULTRA X-ray photoelectron spectrometer equipped with a 165 mm hemispherical electron energy analyzer. The incident radiation was the Mg Kα X-ray line (1253.6 eV) with a source power of 180 W (15 kV, 12 mA). The analysis chamber was maintained at a steady base pressure of $<6 \times 10^{-9}$ Torr during sample analysis. Survey scans of up to 1100 eV were carried out at an analyzer pass energy of 160 eV with 1.0 eV steps and a dwell time of 300 ms. Multiplexed high resolution scans of the Ga(3d), C(1s), As(3d), and N(1s) regions were taken at a pass energy of 40 eV with 0.1 eV steps and a dwell time of 60 ms. The survey and high resolution spectra were obtained with averages of 5 and 50 scans, respectively. The C(1s) peak at 284.8 eV was set as a reference for all XPS peak positions to compensate for energy shifts due to the spectrometer work function.

Synthesis of CdSe QDs. Trioctylphosphine oxide (TOPO)-passivated CdSe spherical nanocrystals were synthesized from well-established solvothermal methods.[41,42] A 250 mg portion of CdO with 2.85 g hexadecylamine, 1.15 g TOPO, and 1.09 g tetradecylphosphic acid were degassed under reduced pressure at 110 °C for 1 h. Then, under nitrogen, the solution was heated to 300 °C until it became optically clear. A 0.5 g portion of tri-*n*-butylphosphine (TBP) was injected and the temperature was reduced to 260 °C; 0.8 g of a 10% by weight Se powder in TBP solution was then quickly injected. When the desired size was reached, the flask was cooled down to 60 °C and 10 g of nonanoic acid was added. Methanol was used to clean the solution and the nanocrystals were subsequently resuspended in toluene. Cleaning with methanol was repeated three times. Exchange of surfactant group from TOPO to water-soluble group was performed as follows.[43] First, 20 mg of 16-mercaptohexadecanoic acid (16-MHA) was dissolved in 15 mL of methanol. The pH of the solution was adjusted to 10−11 using tetramethylammonium hydroxide and 20 mg of CdSe nanocrystals were added to this solution. The mixture was refluxed under nitrogen atmosphere for 6 h. To clean the nanocrystals, a mixture of ethyl acetate and ether was used to precipitate the particles which could then be resuspended in methanol. Subsequent cleanings used only ethyl acetate to precipitate the particles. After the final cleaning, the 16-MHA-passivated CdSe were resuspended in water. The particle size was determined by TEM (see Supporting Information).

Synthesis of Gold and Silver Nanoparticles. Two types of particles were investigated in this study, Au nanoparticles and Ag nanoprisms. Au nanoparticles were prepared by reducing $HAuCl_4$ (Alfa Aesar, 99.99% purity) with sodium citrate.[44] The size of the citrate-stabilized gold NPs was determined to be ~18 nm in diameter based on the maximum surface plasmon absorbance in the UV−visible spectra (USB-ISS-UV/vis, Ocean Optics Inc.) at 523 nm. AFM images of isolated Au particles also confirmed the size to be 18 ± 2 nm. The Ag nanoprisms, were synthesized by first creating spherical silver NPs by the reduction of $AgNO_3$ (Sigma, 99+% purity) with $NaBH_4$ in an ice bath.[45] Here, 1 mL of 10 mM $AgNO_3$ in water was injected into 99 mL of 1 mM $NaBH_4$ and 0.3 mM sodium citrate aqueous solution. The color of this mixed solution turned to yellow immediately (Figure S2A) and was kept stirring in an ice bath for 30 min. The photochemical shape conversion of spherical Ag NPs into flat nanoprisms was carried out by exposure to a white fluorescent lamp (15 W) for ~72 h with a sample-source distance of ~5 cm. The color of the Ag NPs solution changed from yellow to green (Figure S2A) gradually during the period of illumination. The average edge length and thickness of triangular Ag nanoprisms measured by TEM (*vide infra*) were 100 ± 20 nm and 12 ± 3 nm, respectively (Figure S2C). Approximately 50% of the Ag nanoparticles were found to be completely converted to nanoprisms.

Patterning of Metal Nanoparticles. Various approaches were explored for the attachment of Au and Ag nanoparticles to the GaAs surface (see Supporting Information) with the optimal procedure described here. Briefly, the synthesized MNPs were bound to an oxidized GaAs surface by attachment to a patterned layer of APTES on the surface (*vide supra*). Patterned arrays of the APTES SAMs were created on the oxidized GaAs surface by photolithography. Here, a grid pattern was generated on the GaAs surface using a TEM grid (T2000-Cu, Electron Microscopy Inc.) as a shadow mask. The TEM grid was placed on top of the APTES-modified GaAs and the mask/substrate framework was exposed to UV/ozone (λ_{em} = 185 and 254 nm) at a distance of ~1 cm away from the sample for 15 min. After selective photo-oxidation of the APTES SAM, the TEM grid was removed from the surface and the substrate was rinsed with ethanol and then immersed into a 5 mM solution of *n*-octadecyltrimethoxysilane (OTMS) in toluene for 4 h, allowing the OTMS SAM to grow and fill in the exposed GaAs regions. This resulted in a patterned array of hydrophobic and hydrophilic regions on the surface. After patterning, the surfaces were rinsed in sequence with toluene, ethanol, and water, followed by a soaking in one of the citrate-stabilized Au or Ag nanoparticle solutions for 12 h to allow for attachment of the MNPs onto APTES SAMs by electrostatic attraction. Following nanoparticle attachment, the samples were rinsed copiously with water to remove any Au or Ag NPs nonspecifically bound to the hydrophobic regions of the surface.

Layer-by-layer Deposition of Polymers. To control separation distance between the patterned MNPs and the CdSe, a polymer spacer formed by layer-by-layer assembly was used. Here, a positively charged polymer solution was prepared by adding 0.5 M NaCl to an aqueous 5 μL/mL poly(diallyldimethylammonium chloride) (PDADMAC) (Aldrich, 20 wt % in water, M_w = 10 0000−200 000) solution. For the negatively charged polymer solution, an aqueous solution of 1 mg/mL poly(sodium 4-styrenesulfonate) (PSS) (Aldrich, M_w = 70 000) containing 0.5 M NaCl was prepared. To create different thicknesses of polymer layers, the patterned metal arrays on GaAs (carrying net negative charge) were immersed into the PDADMAC solution for 30

min to allow for full adsorption of a single layer. The substrate was then rinsed liberally with water and followed by dipping into the PSS solution for the second layer polymer adsorption. For multilayer deposition, this cycle was repeated, with the outermost layer always terminating in a positive layer of PDADMAC to allow for the further attachment of negatively charged 16-mercaptohexadecanoic acid terminated CdSe QDs.

Sample Imaging. AFM images were acquired with a combined confocal fluorescence/atomic force microscope (WITec Alpha300 R, Germany) under ambient conditions (24 ± 2 °C). All AFM images were acquired in tapping mode using commercially available aluminum-coated silicon AFM tips from Nanoscience Instrument (Phoenix, AZ) with nominal tip radii of less than 10 nm and nominal spring constants of 48 N/m. Images were acquired at a resolution of 512 × 512 lines at a scan rate of ~1 Hz. The photoluminescence spectra were collected using an Ar ion laser at 488 nm (~70 $\mu W/\mu m^2$) as the excitation source with a typical integration time of 36 ms/pixel. A Nikon 100× (0.9 NA) objective was utilized for imaging and spectral data acquisition and the laser was focused to a spot size of ~1 μm^2. The spectral data were acquired with an Acton triple grating spectrometer with an Andor Peltier cooled (−66 °C) CCD detector. High resolution images are obtained by integrating the complete photoluminescence spectra for the given region of interest (500−650 nm for the 4 nm CdSe QDs, 550−700 nm for the 5.5 nm CdSe QDs, and 750 − 900 nm for the GaAs) at each image pixel (typically 200 × 200 pixels per image). Scanning electron microscopy (SEM) images were obtained with a Joel 6400 SEM under vacuum. All samples for SEM imaging were modified by Au sputtering to increase the conductivity and decrease the effects of charging. Transmission electron micrographs (TEM) of the synthesized CdSe nanoparticles were acquired using a JEOL 2010 transmission electron microscope at an acceleration voltage of 200 kV. Samples were prepared using copper grids from Ted Pella. A drop of CdSe solution, in toluene, was dropped onto the grid and allowed to evaporate at room temperature (see Supporting Information).

Acknowledgment. J.D.B. gratefully acknowledges support for this research from the Texas Higher Education Coordinating Board—Norman Hackerman Advanced Research Program (010366-0006-2006), The Robert A. Welch Foundation (A-1620), the TAMU Energy Resource Program, and the National Science Foundation (CHE-0755207). The authors are also very grateful to Dr. Qing-Sheng Liu at Texas A&M University for help in conducting the TEM measurements in this work.

Supporting Information Available: TEM images of CdSe QDs. UV−visible absorption spectra, TEM images of the MNPs, and optical images of the silver nanoparticle solutions. GaAs surface functionalization procedures tested. Calculations of R_Q for FRET and NSET mechanisms. This material is available free of charge *via* the Internet at http://pubs.acs.org.

REFERENCES AND NOTES

1. Reinhard, B. M.; Siu, M.; Agarwal, H.; Alivisatos, A. P.; Liphardt, J. Calibration of Dynamic Molecular Rulers Based on Plasmon Coupling between Gold Nanoparticles. *Nano Lett.* **2005**, *5*, 2246–2252.
2. Sönnichsen, C.; Reinhard, B. M.; Liphardt, J.; Alivisatos, A. P. A Molecular Ruler Based on Plasmon Coupling of Single Gold and Silver Nanoparticles. *Nat. Biotechnol.* **2005**, *23*, 741–745.
3. Zhang, X.; Zhao, J.; Whitney, A. V.; Elam, J. W.; Duyne, R. P. V. Ultrastable Substrates for Surface-Enhanced Raman Spectroscopy: Al_2O_3 Overlayers Fabricated by Atomic Layer Deposition Yield Improved Anthrax Biomarker Detection. *J. Am. Chem. Soc.* **2006**, *128*, 10304–10309.
4. Lyandres, O.; Shah, N. C.; Yonzon, C. R.; Walsh, J. T., Jr.; Glucksberg, M. R.; Duyne, R. P. V. Real-Time Glucose Sensing by Surface-Enhanced Raman Spectroscopy in Bovine Plasma Facilitated by a Mixed Decanethiol/Mercaptohexanol Partition Layer. *Anal. Chem.* **2005**, *77*, 6134–6139.
5. Hecker, N. E.; Hopfel, R. A.; Sawaki, N.; Maier, T.; Strasser, G. Surface Plasmon-Enhanced Photoluminescence from a Single Quantum Well. *Appl. Phys. Lett.* **1999**, *75*, 1577–1579.
6. Shimizu, K. T.; K.Woo, W.; Fisher, B. R.; Eisler, H. J.; Bawendi, M. G. Surface-Enhanced Emission from Single Semiconductor Nanocrystals. *Phys. Rev. Lett.* **2002**, *89*, 117401-1–117401-4.
7. Kulakovich, O.; Strekal, N.; Yaroshevich, A.; Maskevich, S.; Gaponenko, S.; Nabiev, I.; Woggon, U.; Artemyev, M. Enhanced Luminescence of CdSe Quantum Dots on Gold Colloids. *Nano Lett.* **2002**, *2*, 1449–1452.
8. Okamoto, K.; Niki, I.; Shvartser, A.; Narukawa, Y.; Mukai, T.; Scherer, A. Surface-Plasmon-Enhanced Light Emitters Based on InGaN Quantum Wells. *Nat. Mater.* **2004**, *3*, 601–605.
9. Biteen, J. S.; Pacifici, D.; Lewis, N. S.; Atwater, H. A. Enhanced Radiative Emission Rate and Quantum Efficiency in Coupled Silicon Nanocrystal-Nanostructured Gold Emitters. *Nano Lett.* **2005**, *5*, 1768–1773.
10. Pompa, P. P.; Martiradonna, L.; Torre, A. D.; Sala, F. D.; Manna, L.; Vittorio, M. D.; Calabi, F.; Cingolani, R.; Rinaldi, R. Metal-Enhanced Fluorescence of Colloidal Nanocrystals with Nanoscale Control. *Nat. Nanotechnol.* **2006**, *1*, 126–130.
11. Murphy, C. J. Plasmons Spring into Action. *Nat. Mater.* **2007**, *6*, 259–260.
12. Tao, Y. T. Structural Comparison of Self-Assembled Monolayers of *n*-Alkanoic Acids on the Surfaces of Silver, Copper, and Aluminum. *J. Am. Chem. Soc.* **1993**, *115*, 4350–4358.
13. Smith, E. L.; Porter, M. D. Structure of Monolayers of Short Chain *n*-Alkanoic Acids ($CH_3(CH_2)_nCOOH$, $n = 0-9$) Spontaneously Adsorbed from the Gas Phase at Silver as Probed by Infrared Reflection Spectroscopy. *J. Phys. Chem.* **1993**, *97*, 8032–8038.
14. Ghosh, S. K.; Pal, A.; Kundu, S.; Nath, S.; Pal, T. Fluorescence Quenching of 1-Methylaminopyrene near Gold Nanoparticles: Size Regime Dependence of the Small Metallic Particles. *Chem. Phys. Lett.* **2004**, *395*, 366–372.
15. Jin, R.; Cao, Y.; Mirkin, C. A.; Kelly, K. L.; Schatz, G. C.; Zheng, J. G. Photoinduced Conversion of Silver Nanospheres to Nanoprisms. *Science* **2001**, *294*, 1901–1903.
16. Noguez, C. Surface Plasmons on Metal Nanoparticles: The Influence of Shape and Physical Environment. *J. Phys. Chem. C* **2007**, *111*, 3806–3819.
17. Su, K.-H.; Wei, Q.-H.; Zhang, X.; Mock, J. J.; Smith, D. R.; Schultz, S. Interparticle Coupling Effects on Plasmon Resonances of Nanogold Particles. *Nano Lett.* **2003**, *3*, 1087–1090.
18. Biteen, J. S.; Lewis, N. S.; Atwater, H. A.; Mertens, H.; Polman, A. Spectral Tuning of Plasmon-Enhanced Silicon Quantum Dot Luminescence. *Appl. Phys. Lett.* **2006**, *88*, 131109-1–131109-3.
19. Mertens, H.; Biteen, J. S.; Atwater, H. A.; Polman, A. Polarization-Selective Plasmon-Enhanced Silicon Quantum-Dot Luminescence. *Nano Lett.* **2006**, *6*, 2622–2625.
20. Zimnitsky, D.; Jiang, C. Y.; Xu, J.; Lin, Z. Q.; Zhang, L.; Tsukruk, V. V. Photoluminescence of a Freely Suspended Monolayer of Quantum Dots Encapsulated into Layer-by-Layer Films. *Langmuir* **2007**, *23*, 10176–10183.
21. Caruso, F.; Lichtenfeld, H.; Donath, E.; Möhwald, H. Investigation of Electrostatic Interactions in Polyelectrolyte Multilayer Films: Binding of Anionic Fluorescent Probes to Layers Assembled onto Colloids. *Macromolecules* **1999**, *32*, 2317–2328.
22. Tian, Z.-Q.; Ren, B.; Li, J.-F.; Yang, Z.-L. Expanding Generality of Surface-Enhanced Raman Spectroscopy with Borrowing SERS Activity Strategy. *Chem. Commun.* **2007**, *34*, 3514–3534.
23. Kamat, P. V.; Shanghavi, B. Interparticle Electron Transfer in Metal/Semiconductor Composites. Picosecond Dynamics of CdS-Capped Gold Nanoclusters. *J. Phys. Chem. B* **1997**, *101*, 7675–7679.

24. Walters, R. J.; Bourianoff, G. I.; Atwater, H. A. Field-Effect Electroluminescence in Silicon Nanocrystals. *Nat. Mater.* **2005**, *2*, 143–146.
25. Bagalkot, V.; Zhang, L.; Levy-Nissenbaum, E.; Jon, S.; Kantoff, P. W.; Langer, R.; Farokhzad, O. C. Quantum Dot-Aptamer Conjugates for Synchronous Cancer Imaging, Therapy, and Sensing of Drug Delivery Based on Bi-fluorescence Resonance Energy Transfer. *Nano Lett.* **2007**, *7*, 3065–3070.
26. Xu, C. S.; Kim, H.; Yang, H.; Hayden, C. C. Multiparameter Fluorescence Spectroscopy of Single Quantum Dot-Dye FRET Hybrids. *J. Am. Chem. Soc.* **2007**, *129*, 11008–11009.
27. Pons, T.; Medintz, I. L.; Sapsford, K. E.; Higashiya, S.; Grimes, A. F.; English, D. S.; Mattoussi, H. On the Quenching of Semiconductor Quantum Dot Photoluminescence by Proximal Gold Nanoparticles. *Nano Lett.* **2007**, *7*, 3157–3164.
28. Kooij, E. S.; Brouwer, E. A. M.; Wormeester, H.; Poelsema, B. Ionic Strength Mediated Self-Organization of Gold Nanocrystals: An AFM Study. *Langmuir* **2002**, *18*, 7677–7682.
29. Bek, A.; Jansen, R.; Ringler, M.; Mayilo, S.; Klar, T. A.; Feldmann, J. Fluorescence Enhancement in Hot Spots of AFM-Designed Gold Nanoparticle Sandwiches. *Nano Lett.* **2008**, *8*, 485–490.
30. Lakowicz, J. R. *Principles of Fluorescence Spectroscopy,* 3 ed.; Springer: New York, 2006.
31. Medintz, I. L.; Mattoussi, H. Quantum Dot-based Resonance Energy Transfer and Its Growing Application in Biology. *Phys. Chem. Chem. Phys.* **2009**, *11*, 17–45.
32. Anger, P.; Bharadwaj, P.; Novotny, L. Enhancement and Quenching of Single-Molecule Fluorescence. *Phys. Rev. Lett.* **2006**, *96*, 113002-1–113002-4.
33. Yun, C. S.; Javier, A.; Jennings, T.; Fisher, M.; Hira, S.; Peterson, S.; Hopkins, B.; Reich, N. O.; Strouse, G. F. Nanometal Surface Energy Transfer in Optical Rulers, Breaking the FRET Barrier. *J. Am. Chem. Soc.* **2005**, *127*, 3115–3119.
34. Govorov, A. O.; Lee, J.; Kotov, N. A. Theory of Plasmon-Enhanced Förster Energy Transfer in Optically Excited Semiconductor and Metal Nanoparticles. *Phys. Rev. B* **2007**, *76*, 125308-1–125308-16.
35. Jennings, T. L.; Schlatterer, J. C.; Singh, M. P.; Greenbaum, N. L.; Strouse, G. F. NSET Molecular Beacon Analysis of Hammerhead RNA Substrate Binding and Catalysis. *Nano Lett.* **2006**, *6*, 1318–1324.
36. Jennings, T. L.; Singh, M. P.; Strouse, G. F. Fluorescent Lifetime Quenching near $d = 1.5$ nm Gold Nanoparticles: Probing NSET Validity. *J. Am. Chem. Soc.* **2006**, *128*, 5462–5467.
37. Thomas, M.; Greffet, J.-J.; Carminati, R.; Arias-Gonzalez, J. R. Single-Molecule Spontaneous Emission close to Absorbing Nanostructures. *Appl. Phys. Lett.* **2004**, *85*, 3863–3865.
38. Chen, Y.; Munechika, K.; Ginger, D. S. Dependence of Fluorescence Intensity on the Spectral Overlap between Fluorophores and Plasmon Resonant Single Silver Nanoparticles. *Nano Lett.* **2007**, *7*, 690–696.
39. Kühn, S.; Håkanson, U.; Rogobete, L.; Sandoghdar, V. Enhancement of Single-Molecule Fluorescence Using a Gold Nanoparticle as an Optical Nanoantenna. *Phys. Rev. Lett.* **2006**, *97*, 017402−1−017402−1-4.
40. Jun, Y.; Zhu, X.-Y.; Hsu, J. W. P. Formation of Alkanethiol and Alkanedithiol Monolayers on GaAs(001). *Langmuir* **2006**, *22*, 3627–3632.
41. Peng, Z. A.; Peng, X. Formation of High-Quality CdTe, CdSe, and CdS Nanocrystals Using CdO as Precursor. *J. Am. Chem. Soc.* **2001**, *123*, 183–184.
42. Reiss, P.; Bleuse, J.; Pron, A. Highly Luminescent CdSe/ZnSe Core/Shell Nanocrystals of Low Size Dispersion. *Nano Lett.* **2002**, *2*, 781–784.
43. Aldana, J.; Wang, Y. A.; Peng, X. Photochemical Instability of CdSe Nanocrystals Coated by Hydrophilic Thiols. *J. Am. Chem. Soc.* **2001**, *123*, 8844–8850.
44. Frens, G. Controlled Nucleation for the Regulation of the Particle Size in Monodisperse Gold Suspensions. *Nat. Phys. Sci.* **1973**, *241*, 20–22.
45. Lee, P. C.; Meisel, D. Adsorption and Surface-Enhanced Raman of Dyes on Silver and Gold Sols. *J. Phys. Chem.* **1982**, *86*, 3391–3395.